

# The magnetization-driven random field Ising model at $T = 0$

Xavier Illa,<sup>1,\*</sup> Martin-Luc Rosinberg,<sup>2</sup> Prabodh Shukla,<sup>3</sup> and Eduard Vives<sup>1</sup>

<sup>1</sup> *Departament d'Estructura i Constituents de la Matèria, Universitat de Barcelona  
Diagonal 647, Facultat de Física, 08028 Barcelona, Catalonia*

<sup>2</sup> *Laboratoire de Physique Théorique de la Matière Condensée,*

*Université Pierre et Marie Curie, 4 Place Jussieu, 75252 Paris, France*

<sup>3</sup> *Physics Department, North Eastern Hill University, Shillong 793003, India*

(Dated: March 24, 2021)

We study the hysteretic evolution of the random field Ising model (RFIM) at  $T = 0$  when the magnetization  $M$  is controlled externally and the magnetic field  $H$  becomes the output variable. The dynamics is a simple modification of the single-spin-flip dynamics used in the  $H$ -driven situation and consists in flipping successively the spins with the largest local field. This allows to perform a detailed comparison between the microscopic trajectories followed by the system with the two protocols. Simulations are performed on random graphs with connectivity  $z = 4$  (Bethe lattice) and on the 3-D cubic lattice. The same internal energy  $U(M)$  is found with the two protocols when there is no macroscopic avalanche and it does not depend on whether the microscopic states are stable or not. On the Bethe lattice, the energy inside the macroscopic avalanche also coincides with the one that is computed analytically with the  $H$ -driven algorithm along the unstable branch of the hysteresis loop. The output field, defined here as  $\Delta U/\Delta M$ , exhibits very large fluctuations with the magnetization and is not self-averaging. Relation to the experimental situation is discussed.

PACS numbers: 75.60.Ej, 75.50.Lk, 81.30.Kf, 81.40.Jj

## I. INTRODUCTION

The random-field Ising model (RFIM) is one of the simplest model to study the combined effects of interaction and disorder in many-body systems. In particular, the response of the RFIM to a slowly varying magnetic field at zero temperature[1] illustrates the athermal dynamical behavior observed in several experimental systems in condensed matter physics such as disordered ferromagnets, superconductors, martensitic materials, etc. This response is characterized by avalanches and rate-independent hysteresis. Recently, the model has also been transposed to the context of finance and human behavior[2].

The aim of the present work is to study the  $T = 0$  RFIM in a situation that has not been considered so far, when one varies the overall magnetization and not the magnetic field (which then becomes a derived quantity that we will call the “output” field). More generally, we want to describe the behavior of athermal systems under control of the *extensive* variable conjugated to the intensive force. This concerns for instance the stress-strain curves in shape-memory materials that are usually obtained by controlling the deformation of the sample and measuring the induced stress[3]. One also uses a feedback control that imposes a constant variation of the magnetic flux in the case of ferromagnets with a very steep magnetization curve[4].

For a system at equilibrium, it is of course equivalent to control the force or the conjugated variable: the sys-

tem follows a well-defined curve which corresponds to the minimum of the energy or the free-energy. This curve may be continuous or discontinuous, as is the case at a first-order phase transition. The situation is more complicated when thermal fluctuations are too small to overcome the energy barriers and the system remains far from thermodynamic equilibrium on the experimental time scale. It then follows a metastable, history-dependent path, and there is no reason for observing the same behavior with the two protocols. In fact, there is experimental evidence that hysteresis loops obtained by varying extensive variables display bending-back trajectories (with a so-called yield point), and large fluctuations in the measured force (or field)[4, 5].

In order to simulate this situation with the  $T = 0$  RFIM, one needs to introduce a dynamical rule that states how to flip the spins as the magnetization is changed. There are of course different ways of locally minimizing the energy and the choice for the dynamics is not unique, even if one imposes a deterministic rule so to get the same result when repeating the simulation. In this work, we propose to modify the standard single-spin-flip dynamics in a *minimal* way, so that the new dynamics may be considered as the “magnetization-driven” version of the dynamics used in the field-driven case[6]. The main advantage is that there is a close connection between the microscopic trajectories followed by the system with the two protocols and the results for the macroscopic quantities (for instance the internal energy) can be readily compared,

Another and more delicate issue concerns the definition of the magnetic field as an output variable. The solution that we adopt is again very simple but cannot be considered as fully satisfactory. In another recent work[7], a

---

\*Electronic address: xit@ecm.ub.es

different approach was proposed, extending the study to finite temperatures so to define the field as a Lagrange multiplier. Comparison between these two approaches is discussed below. Part of our study is performed on a Bethe lattice with connectivity  $z = 4$  (or, equivalently, on random graphs with the same connectivity). This is to benefit from the fact that an almost complete analytical description is available in the field-driven case[8, 9, 10]. Comparing our simulation data with these exact results will help in understanding the similarities and differences between the two protocols.

In section II, we review the model in the usual field-driven situation and introduce the modifications in the dynamics so to describe the magnetization-driven case. The simulation results for the Bethe lattice are discussed in section III and those for the 3-D cubic lattice in section IV. We summarize our main findings and conclude in section V.

## II. MODEL

The RFIM with single-spin-flip local relaxation dynamics was specifically introduced for studying the  $H$ -driven situation. It is thus usually formulated from a microscopic Hamiltonian  $\mathcal{H}$  that corresponds to the magnetic enthalpy. For the present study, it is convenient to first introduce the internal energy  $\mathcal{U}$ :

$$\mathcal{U} = - \sum_{\langle i,j \rangle} S_i S_j - \sum_i h_i S_i \quad (1)$$

where  $S_i = \pm 1$  are spin variables defined on the sites  $i = 1, \dots, N$  of a lattice and the first sum extends over all nearest-neighbor pairs (the coupling constant is taken as the energy unit and set to unity). The random fields  $h_i$  are i.i.d. variables sampled from the Gaussian distribution  $\rho(h) = \exp(-h^2/2\sigma^2)/\sqrt{2\pi}\sigma$  with standard deviation  $\sigma$ . The enthalpy  $\mathcal{H}$  is then defined as

$$\mathcal{H} = \mathcal{U} - HM \quad (2)$$

where  $M = \sum_i S_i$  is the overall magnetization. In the following, we consider two types of lattice: a 3-D cubic lattice and a Bethe lattice with connectivity  $z = 4$ . In the first case, numerical simulations are performed on finite lattices of size  $N = L \times L \times L$  with periodic boundary conditions. In the second case, they are performed on random graphs with fixed connectivity  $z = 4$  which provide a convenient realization of the Bethe lattice in the thermodynamic limit.

### A. $H$ -driven dynamics

The standard  $H$ -driven dynamics consists in locally minimizing the enthalpy  $\mathcal{H}$ . As the external field  $H$  is changed, each spin is aligned with its total local field

$f_i + H$ , where

$$f_i = \sum_{j/i} S_j + h_i \quad (3)$$

and the summation is over all the  $z$  neighbors  $j$  of  $i$ . A configuration  $\{S_i\}$  is then (meta)stable when all the spins satisfy the condition.

$$S_i = \text{sign}(f_i + H) \quad (4)$$

One usually starts the metastable evolution with  $H = -\infty$  and all spins  $S_i = -1$ .  $H$  is then increased until the total local field vanishes at a certain site. This first occurs for the spin with the largest random field,  $h_i^{max}$ . This spin is then flipped, which in turn changes the local field at the neighbors and may trigger an avalanche of other spin flips. The avalanche stops when a new stable configuration is reached.  $H$  is then increased again until a new spin becomes unstable and the evolution continues until all the spins flip up. The upper half of the hysteresis loop is obtained in a similar way by decreasing the field from  $+\infty$  to  $-\infty$ . Note that the external field  $H$  is kept constant during an avalanche, which corresponds to a complete separation of time scales between the driving mechanism and the internal relaxation of the system (the dynamics is then referred to as ‘‘adiabatic’’). Because the interactions are purely ferromagnetic, the dynamics has also some remarkable properties: it is abelian[9] (the order in which unstable spins are flipped during an avalanche is irrelevant for determining the final state) and it satisfies return-point memory[6]. An important feature is the existence of a critical amount of disorder  $\sigma_c$  below which the hysteresis loops are discontinuous in the thermodynamic limit, the jump in the magnetization corresponding to the occurrence of a macroscopic avalanche[6]. One has  $\sigma_c \approx 2.2$  for the cubic lattice[11, 12] and  $\sigma_c = 1.781258\dots$  for the Bethe lattice with connectivity  $z = 4$ [8].

Fig. 1 shows an example of an  $H$ -driven metastable evolution on a random graph with connectivity  $z = 4$ . For the sake of comparison with the  $M$ -driven protocol that is introduced in the next section, we plot the internal energy per spin  $u = \mathcal{U}/N$  as a function of the magnetization per spin  $m = M/N$  (both quantities being parametrized by the external field  $H$ ). The metastable states  $\{S_i\}_1, \{S_i\}_2, \{S_i\}_3, \dots$  visited by the dynamics are represented by triangles while the dashed lines in-between indicate the avalanches. Note that the total number of states when  $H$  is varied from  $-\infty$  to  $+\infty$  depends on the disorder strength and on the particular realization of the random fields. Typically, there are only a few states when  $\sigma$  is small (most avalanches are large) whereas the number of states approaches its upper limit  $N$  when  $\sigma$  is large.

Finally, we want to stress that the energetic barriers between the metastable states are strictly defined by the dynamics. In fact, the very definition of the metastable states (i.e. the stability rule (4)) cannot be separated

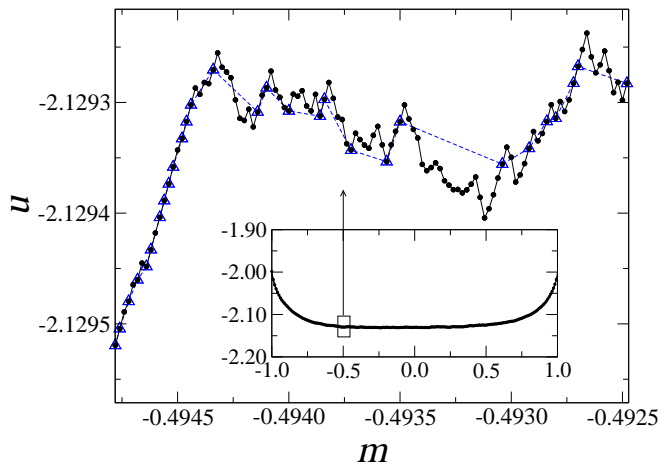


FIG. 1: (Color on line) Comparison between the  $H$ -driven and  $M$ -driven trajectories in the energy-magnetization plane ( $u = \mathcal{U}/N$  is the internal energy per spin). Data correspond to a single disorder realization with  $\sigma = 2$  on a random graph with connectivity  $z = 4$  ( $N = 10^5$ ). The triangles represent the states visited by the  $H$ -driven dynamics which are separated by avalanches (dashed lines). The dots are the states visited by the  $M$ -driven dynamics.

from the use of the single-spin-flip dynamics. It has been shown recently that a slightly better minimization of the enthalpy (obtained by allowing also simultaneous flips of nearest-neighbor spins) yields much thinner hysteresis loops while not changing the critical behavior of the system[13].

### B. $M$ -driven dynamics

We now define an irreversible dynamics for the case where the magnetization of the system is changed externally. There is no external field and the potential that has to be minimized (at least partially) is the internal energy  $\mathcal{U}$ . Our goal is to generate a sequence of states  $\{S_i\}_1, \{S_i\}_2, \{S_i\}_3, \dots$  when  $M$  is increased from  $M = -N$  to  $M = +N$  by elementary steps  $\Delta M = 2$ . As noted in the introduction, we want this dynamics to be as close as possible to the single-spin-flip dynamics used in the  $H$ -driven case. For instance, we require that the two driving mechanisms become equivalent when the spins behave independently and the hysteresis vanishes (either because the coupling constant is zero or  $\sigma \rightarrow \infty$ ). In this limit, one must thus flip, for each value of  $M$ , the spin with the largest random field,  $h_i^{max}$ . In the general case, we propose to use the simplest “extremal” dynamics: the spins are flipped one by one (like in the  $H$ -driven case) and, for each value of  $M$ , one chooses the spin that *most* decreases or, at least, *less* increases the internal energy. This is the spin with the largest local field,  $f_i^{max}$ , and the corresponding change in the energy is  $\Delta\mathcal{U} = -2f_i^{max}$ . After the spin has been flipped, the local fields  $f_i$  at the

neighbors are updated and the same rule is applied until all spins are flipped. One obtains a different sequence of states when starting from  $M = +N$  and decreasing the magnetization, which yields an hysteresis loop. It may be remarked that this new dynamics bears some similarity with the “extremal” dynamics used in simple models of self-organized criticality (see e.g. Ref.[15]). However, in the present case, one never reaches a statistically stationary state because each spin in the system flips only once and  $m$  evolves between  $-1$  and  $+1$ .

By construction, the total number of states visited by the dynamics is now  $N$  and the crucial feature is that this sequence of states contains *all* the  $H$ -driven metastable states as a subsequence. This is due to the abelian property of the  $H$ -driven dynamics and can be easily understood by noticing that i) the two dynamics start with the same initial state (with all  $S_i = -1$  or  $+1$ ), and ii) the spins that are flipped successively within the  $M$ -driven dynamics are either those which trigger an  $H$ -driven avalanche or those which are involved in this avalanche. In other words, the dynamical rule that has been chosen generates a sequence of states that are obtained by flipping *in a certain order* the spins involved in the  $H$ -driven avalanches. This is illustrated in Fig. 1 which shows the sequences of states obtained with the two dynamics in the  $u - m$  plane. One can see that the  $M$ -driven trajectory is a sort of random walk that joins the metastable states belonging to the  $H$ -driven trajectory.

A more problematic (but separate) issue concerns the definition of the output field  $H$  associated to the changes in the magnetization. As will be discussed below in more detail, one difficulty is that many of the states visited by the dynamics are not metastable. This means that it is not possible to find a field that allows for the condition (4) to be satisfied for all spins. This is because the local field  $f_i$  at some spins down is larger than the local field at some spins up (it is easy to see from Eq.(4) that the condition for a microscopic configuration  $\{S_i\}$  to be metastable at some field  $H$  is that  $f_i^{min}$ , the minimum value of the local field among the spins up, is larger than  $f_i^{max}$ , the maximum value of the local field among the spins down). In this respect, the present situation is totally different from the one considered in Ref. [7] where all the states obtained with the  $M$ -driven dynamics are stable. An additional difficulty is that there is no obvious way to define an intensive quantity conjugated to  $M$ , playing the same role as the Lagrange parameter introduced in Ref. [7]. The simple solution that we propose is to define the field in such a way that the work needed to go from the state at  $M$  to the state at  $M + \Delta M$  is minimal. The field thus identifies with the internal force,

$$H(m) \equiv \Delta\mathcal{U}/\Delta M = -f_i^{max}(m). \quad (5)$$

(In order to facilitate the comparison with the  $H$ -driven dynamics we use the same notation for the external and the output field. For the metastable states that are common to the two dynamics, the field defined by Eq. (5)

is exactly the external field at which these states become marginally stable.)

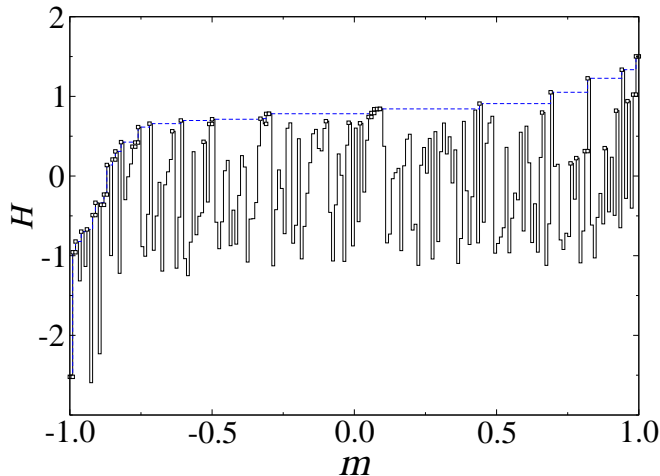


FIG. 2: (Color on line) Comparison between the  $H$ -driven (dashed line) and  $M$ -driven (solid line) trajectories in the field-magnetization plane. Data correspond to a single disorder realization with  $\sigma = 2$  on a random graph with connectivity  $z = 4$  ( $N = 200$ ). The symbols represent the metastable states according to the single-spin-flip dynamics (some of them do not belong to the  $H$ -driven trajectory, as discussed in section III A).

$H(m)$  is not a monotonously increasing function of the magnetization. In fact, as can be seen in Fig. 2 in the case of a very small system, it strongly fluctuates with  $m$ . This is a quite different behavior from the one observed for the magnetization in the  $H$ -driven case. Note however that one can easily deduce the  $H$ -driven trajectory from the  $M$ -driven one (when the magnetization is put on the horizontal axis): it is just the envelope function that tracks the increasing maxima of  $H(m)$ .

A direct consequence of Eq.(5) is that the  $M$ -driven dynamics does not yield any dissipation. Indeed, since the work  $H\Delta M$  is just equal to the variation of the internal energy, the area of any closed loop (that goes back to the same microscopic state) is zero. This is to be contrasted with the situation in the  $H$ -driven case in which the work is larger than  $\Delta\mathcal{U}$  inside the avalanches. Although the experimental hysteresis loops obtained in  $M$ -driven conditions have a much smaller area than the  $H$ -driven loops[4, 5], it is not true that the dissipation is zero. We shall come back to this issue in section V where we discuss some possible modifications in the definition of the field so to avoid this “unphysical” feature.

### C. Fluctuations and self-averaging

The two preceding algorithms allow to simulate a finite system for a given realization  $\{h_i\}$  of the random fields. Comparison with experiments should be performed by

considering the limit  $N \rightarrow \infty$ . It is then desirable that the results are self-averaging, i.e. that they do not depend on a particular realization of the disorder in the thermodynamic limit.

In this respect, the situation is different when one is controlling the external field  $H$  or the magnetization  $M$ . In the former case, one can divide a macroscopic system into a large number of macroscopic subsystems that are all submitted to the *same* external field. Then, according to a standard argument[16], away from criticality, the value of the density of any extensive quantity on the whole system (for instance the magnetization  $M(H)$ ) is equal to the average of the (independent) values of this quantity over the subsystems. According to the central limit theorem, this quantity is distributed with a Gaussian probability distribution and (strongly) self-averaging[17]. On the other hand, in the latter case, one cannot decompose a system into subsystems having the same magnetization and the standard argument does not apply. This implies that i) one must carefully study the behavior of the sample-to-sample fluctuations of an observable as the system size increases so to conclude whether or not this observable is self-averaging, and ii) one must be cautious in giving a physical meaning to the average over disorder.

In the following, we analyze the self-averaging character of an observable  $X$  by performing histograms over many disorder realizations for a given size  $N$ , so to estimate the probability distribution  $P_N(X)$ . We then study the behavior of the variance  $V_X = \langle X^2 \rangle_M - \langle X \rangle_M^2$  as  $N$  increases (here  $\langle \cdot \rangle_M$  denotes the average over disorder at constant  $M$ , which has to be distinguished from  $\langle \cdot \rangle_H$ , the average over disorder at constant  $H$ ).  $X$  is (strongly) self-averaging if  $V_X \sim 1/N$  when  $N \rightarrow \infty$ .

## III. RESULTS FOR THE $z = 4$ BETHE LATTICE

In this section we present the numerical results obtained by simulating the  $M$ -driven dynamics on random graphs with fixed connectivity  $z = 4$ . Since small loops are rare in these graphs (their typical size is of order  $\log N$ ), the results in the large- $N$  limit are expected to converge to the results on a true Bethe lattice, i.e. in the deep interior of a Cayley tree. For the sake of completeness, we first recall the analytical expressions for the average magnetization per spin  $\langle m \rangle_H$  and the average internal energy per spin  $\langle u \rangle_H$  as a function of the external field  $H$ [8, 10]:

$$\langle m \rangle_H = 1 - 2 \sum_{n=0}^z \binom{z}{n} P^{*n} (1 - P^*)^{z-n} p_n \quad (6)$$

$$\begin{aligned} \langle u \rangle_H &= -\frac{1}{2}z + 2 \sum_{n=0}^z \binom{z}{n} P^{*n} [1 - P^*]^{z-n} \\ &\times [n(1 - p_n) + \sigma^2 \rho(z - 2n - H)] \end{aligned} \quad (7)$$

where the quantity  $P^*$  is solution of the equation

$$P^* = \sum_{n=0}^{z-1} \binom{z}{n} P^{*n} (1 - P^*)^{z-1-n} p_n \quad (8)$$

and the functions  $p_n(H)$  ( $n = 0, 1, \dots, z$ ) are integrals of the Gaussian distribution,

$$p_n = \int_{-J(2n-z)-H}^{+\infty} \rho(h) dh. \quad (9)$$

(Eq. (7) is obtained by summing the different contributions to the internal energy computed in Ref.[10].) In the following, we shall also use the expression for the probability (per spin) that an avalanche is initiated when the field is increased from  $H$  to  $H + dH$ . It is defined as  $G(H)dH$  with

$$G(H) = \sum_{n=0}^z \binom{z}{n} P^{*n} [1 - P^*]^{z-n} \rho(z - 2n - H) \quad (10)$$

(this expression corresponds to Eq. (14) in Ref.[9] with  $x = 1$ ).

When computing  $P^*(H)$ , it is important to take into account the fact that Eq. (8) has three real roots in a certain range of  $H$  below  $\sigma_c$ . Then, the magnetization curve obtained from Eq. (6) has an S-shape behavior[8], as illustrated in Fig. 3. The correct physical solution that gives the lower branch of the hysteresis loop corresponds to the smallest root. For a certain value of  $H$ , this root is not real anymore,  $P^*(H)$  jumps to the largest root and there is a discontinuity in the magnetization curve associated to the occurrence of an infinite avalanche. In this context, the intermediate, unstable branch of the S-shape curve (from points A to B in the figure) has no physical meaning (on the other hand, the branch BC can be reached via first-order reversal curves obtained from the descending branch of the hysteresis loop, as noted in Refs.[14, 18]).

#### A. Fraction of stable states along the $H$ -driven and $M$ -driven trajectories

As can be seen in Fig. 2, which corresponds to the simulation of a small system, there are a few states along the  $M$ -driven trajectory that are metastable although they do not belong to the  $H$ -driven subsequence (this could be seen as well in the  $u - m$  diagram since this property does not depend on the definition of the field). Of course, the fact that the state visited by the dynamics is stable or not depends on the disorder realization. It is therefore useful to introduce the quantity  $Q(m)$  that represents the average fraction of states that are stable. As shown in Fig. 3, these additional metastable states appear less and less frequently as the system size increases and there is strong numerical evidence that they completely disappear in the thermodynamic limit. Therefore, when  $N \rightarrow \infty$ ,  $Q(m)$

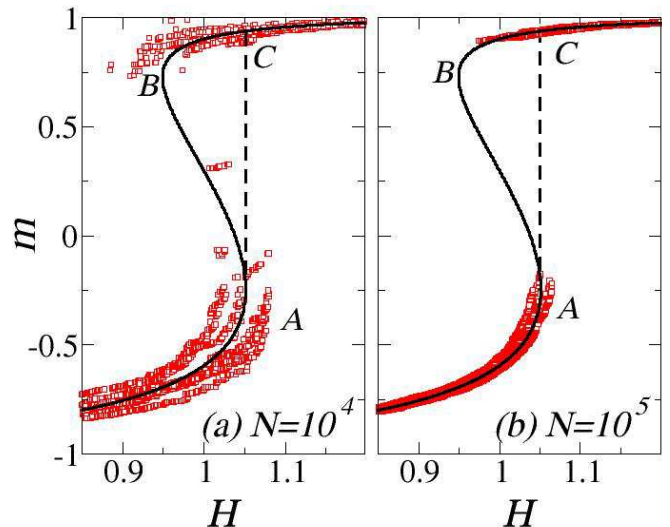


FIG. 3: (Color on line) Ascending branch of the  $H$ -driven hysteresis loop on a Bethe lattice with connectivity  $z = 4$  for  $\sigma = 1.6$ . The solid line corresponds to the solution of Eqs. (6) and (8). The symbols represent all the metastable states obtained along the  $M$ -driven trajectories for 10 disorder realizations on random graphs of size  $N = 10^4$  (a) and  $10^5$  (b).

also represents the average fraction of metastable states along the  $H$ -driven trajectory.

The results of the simulations with the  $M$ -driven dynamics below and above  $\sigma_c$  and different system sizes are shown in Fig. 4. For  $\sigma > \sigma_c$ , it is found that  $Q(m)$  is minimum in the range of  $m$  that corresponds to the steepest part of the  $H$ -driven magnetization curve where the avalanches are the largest. For  $\sigma < \sigma_c$ , the interval where  $Q(m) = 0$  exactly corresponds to the range of the infinite avalanche (including in the portion BC of the magnetization curve, as shown in the inset of Fig. 4). The fact that  $Q(m)$  is *strictly* smaller than 1 (except for  $m = \pm 1$ ) deserves some explanation. With the  $H$ -driven algorithm, there is indeed a certain probability, for a finite system, that a given value of  $M$  corresponds either to a horizontal portion of the magnetization curve (a metastable state) or to a vertical jump (an avalanche). Although the magnetization curve is continuous in the thermodynamic limit (except for the jump below  $\sigma_c$ ), the probability of “hitting” a metastable states remains smaller than 1 when  $N \rightarrow \infty$ . In other words,  $Q(m)$  tracks the random presence of “holes” in the magnetization curve that correspond to the avalanches. This suggests that  $Q(m)$  is related to the probability of having an avalanche between  $H$  and  $H + dH$  (where  $H$  is the field corresponding to  $m$  in the thermodynamic limit). This probability is given by the quantity  $G(H)$  defined by Eq. (10) and the sought relation is

$$Q(m) = 2G(H) \frac{dH}{dm} \quad (11)$$



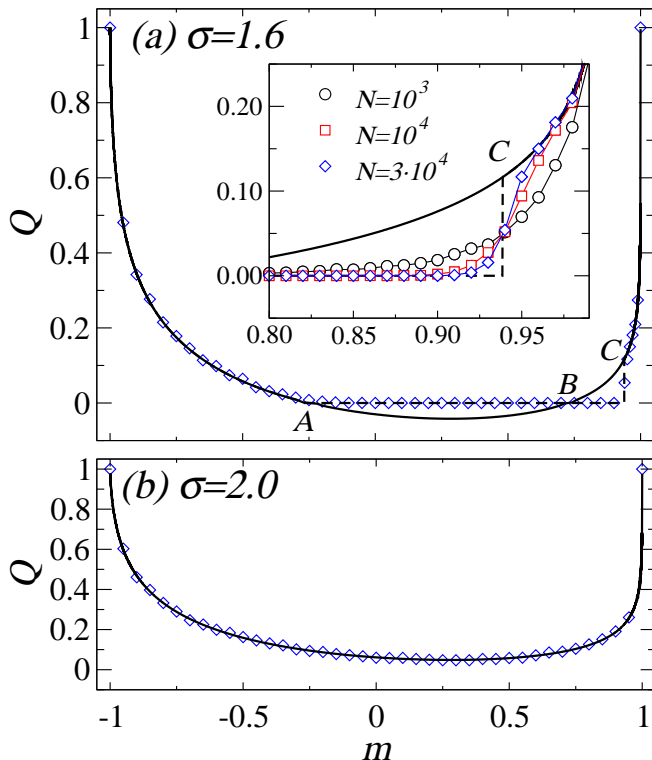


FIG. 4: (Color on line) Fraction  $Q(m)$  of stable states along the ascending branch of the hysteresis loop for a Bethe lattice with  $z = 4$ . The points A, B and C are the same as in Fig. 3. The symbols are the results of the numerical simulation of the  $M$ -driven algorithm. The solid line corresponds to the analytical expression (11) and the dashed line indicates the infinite avalanche below  $\sigma_c$ . The inset in (a) shows that  $Q(m)$  converges to 0 between the points B and C in the thermodynamic limit. Simulation data, indicated by different symbols are joined by guides to the eye.

where  $dH/dm$  is the inverse slope of the magnetization curve in the thermodynamic limit, a quantity that is easily computed from Eq. (6). One can see in Fig. 4 that the agreement between the simulations and the analytical formula is indeed very good. The proof of Eq. (11) relies on the assumption that the occurrence of avalanches (as  $H$  is monotonously increasing) corresponds to a non-stationary Poisson process[6]. For a finite system of size  $N$ , an avalanche then occurs in the interval  $dH$  with a rate  $dP/dH = NG(H)$  (recall that  $G(H)dH$ , as calculated in Ref.[9], is a probability per spin). The mean range of stability  $\langle\Delta H\rangle_H$  of a metastable state before an avalanche occurs is given by the inverse of the rate, i.e.

$$\langle\Delta H\rangle_H \sim \frac{1}{NG(H)} \quad (12)$$

(Note that this quantity becomes infinitesimal in the thermodynamic limit.) Since only metastable states contribute to the variation of  $H$  in the interval  $M, M+2$  (the field is kept constant during an avalanche), the average

slope of the magnetization curve in the thermodynamic limit is given by

$$\frac{dH}{dm} = Q(m) \lim_{N \rightarrow \infty} N \frac{\langle\Delta H\rangle_H}{\Delta M} \quad (13)$$

which yields Eq. (11).

It is interesting to remark that Eq. (11) gives a finite, positive value of  $Q(m)$  between points B and C in Fig. 4(a) when one computes  $m(H)$  using the largest root of Eq. (8). Indeed, as already noted, this part of the  $H$ -driven hysteresis loop can be reached by an appropriate field history starting from saturation: this implies that the fraction of metastable states is not zero. On the other hand, one gets a meaningless negative value for  $Q(m)$  between points A and B and the correct physical result  $Q(m) = 0$ , that states that all configurations are unstable, is recovered by setting  $dm/dH \rightarrow \infty$  in Eq. (11).

## B. Internal energy

We now discuss the simulation results for the internal energy per spin  $u(m)$ . In Fig. 5, we plot on a log-log scale the variance  $V_u(m) = \langle u(m)^2 \rangle_M - \langle u(m) \rangle_M^2$  for selected values of  $m$  as a function of the system size  $N$ . Both above and below  $\sigma_c$ , it is found that  $V_u(m)$  decrease like  $1/N$ , showing that the energy is a strongly self-averaging quantity, a result that is not *a priori* obvious. Accordingly, we shall now use the average value of  $u(m)$  to compare with the exact results obtained with the  $H$ -driven dynamics in the thermodynamic limit, although  $\langle u(m) \rangle_M$  may not be a well-defined physical quantity, as remarked above. Rather, this must be considered as a convenient way of suppressing sample-to-sample fluctuations.

The comparison is performed in Fig. 6 where  $\langle u(m) \rangle_H$  is obtained by plotting  $\langle u \rangle_H$  as a function of  $\langle m \rangle_H$ , the field  $H$  being considered as a parameter (see also Fig. 1). When  $\sigma < \sigma_c$ , there is a jump in the magnetization and the corresponding discontinuity in  $\langle u(m) \rangle_H$  is represented by a dashed line, the solid line representing the internal energy along the intermediate, unstable part of the magnetization curve. It can be seen that the behavior of  $u(m)$  changes with  $\sigma$ . For large disorder, the energy has a “double well” structure whereas there is a single well when the disorder is small. The change in the behavior occurs at  $\sigma \simeq 2.0$  and is therefore not related to the critical value of the disorder at which the discontinuity in the  $H$ -driven magnetization curve disappears. Note moreover that the curves are not symmetric with respect to  $m = 0$ : there is indeed hysteresis when the magnetization is increased from  $-1$  or decreased from  $+1$ .

The most remarkable feature in Fig. 6 is that the average internal energy obtained with the  $M$ -driven algorithm appears to coincide with the analytical curve obtained from Eq. (7) in the thermodynamic limit *even* when  $m$  is in the range of the macroscopic avalanche for  $\sigma < \sigma_c$  (the agreement is better than  $10^{-3}$  for  $N = 10^4$ ).

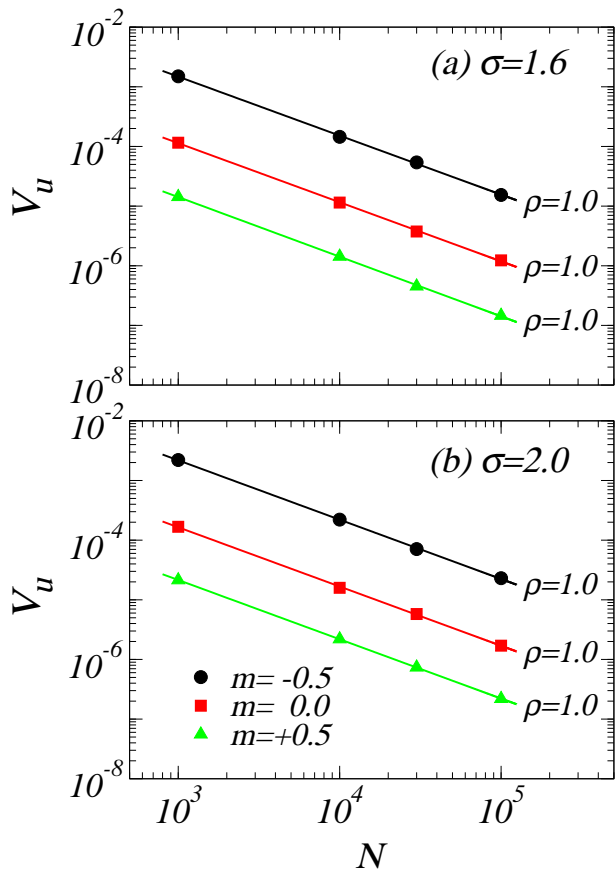


FIG. 5: (Color on line) Variance  $V_u(m)$  of the internal energy per spin  $u(m)$  on random graphs with connectivity  $z = 4$  for selected values of  $m$  as a function of system size. The number of disorder realizations is  $10^4$ . For the sake of clarity, the variances for  $m = 0$  and  $m = 0.5$  are divided by 10 and 100, respectively. The lines are fits to the form  $V_u(m) \sim N^{-\rho}$ , yielding  $\rho \simeq 1.0$  in all cases.

Since this is a surprising result, we have carefully checked the behavior as a function of the system size (note incidentally that finite-size effects are not negligible in the  $H$ -driven case as well: this is an issue that has not yet been investigated, as far as we know).

When all avalanches are of microscopic size, the coincidence of the energy along the two trajectories is due to the fact that the stable states before and after the avalanche (and therefore all the unstable states in-between) differ only by a finite (i.e., non-extensive) number of spin-flips. Accordingly, the energy of these states cannot differ by an extensive quantity and one has

$$\langle u(m) \rangle_M = \langle u(m) \rangle_M^{stable} = \langle u(m) \rangle_M^{unstable} \quad (14)$$

in the thermodynamic limit, as can be checked numerically. Moreover, since both the energy and the magnetization are self-averaging quantities, the averages at fixed

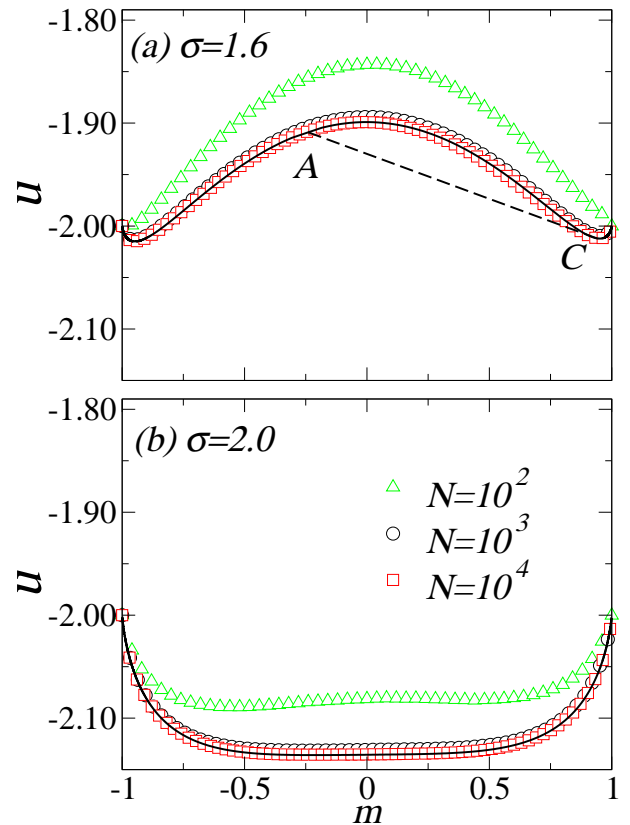


FIG. 6: (Color on line) Average internal energy per spin on the Bethe lattice with  $z = 4$  below and above  $\sigma_c$ . The symbols are the results of the simulation of the  $M$ -driven algorithm on random graphs of different sizes with an average over  $10^4$  disorder realizations. The solid line corresponds to the analytical expression given by Eq. (7). The dashed line indicates the discontinuity associated to the infinite avalanche for  $\sigma < \sigma_c$ .

$m$  or fixed  $H$  yield the same result. Therefore,

$$\langle u(m) \rangle_H \equiv \langle u(m) \rangle_H^{stable} = \langle u(m) \rangle_M^{stable} = \langle u(m) \rangle_M. \quad (15)$$

It is more surprising that the equality  $\langle u(m) \rangle_H = \langle u(m) \rangle_M$  is also satisfied *inside* the macroscopic avalanche if one uses the “unphysical” root of Eq. (8) to compute  $\langle u(m) \rangle_H$  along the unstable branch of the  $H$ -driven magnetization curve. We have no obvious explanation for this result but we want to stress that it crucially depends on the order in which the spins are flipped during an avalanche. Indeed, as illustrated in Fig. 7, a different curve  $\langle u(m) \rangle_M$  is obtained if one decides for instance to flip the spin that *less* decreases the energy. Therefore, the  $M$ -driven dynamics that has been chosen is precisely the one that yields agreement with the analytical solution computed in Ref. 10. This suggests that behind the probabilistic computation in Ref. 8 there is perhaps some hidden minimization principle that fixes unambiguously the trajectory along the unstable branch.

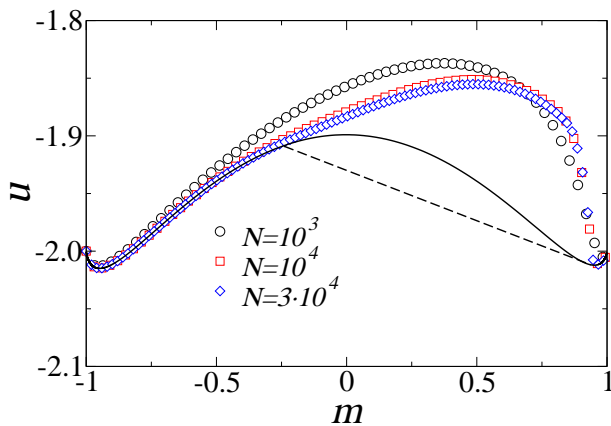


FIG. 7: (Color on line) Same as Fig. 6(a) when, inside an avalanche, one flips the spin that less decreases the energy.

### C. Statistical behavior of the output field

As illustrated by Figs. 2 and 8, the output field  $H(m)$  defined by Eq. (5) displays a sporadic, discontinuous behavior with magnetization. When a spin flips, the local field at the neighbors is changed by  $\pm 2$ , and this is indeed the approximate size of the fluctuations observed in Fig. 8. This of course does not depend on the system size and the same behavior should be observed in the thermodynamic limit. We shall come back to this important issue in section V. Another consequence of the definition of the field as an extremal quantity is that it exhibits large sample-to-sample fluctuations. In fact, it is found that the variance does not decrease with  $N$ , which means that each sample behave differently, even in the thermodynamic limit. It is however instructive to study in detail the probability distribution  $P_N(H; m)$  for different values of  $m$  above and below  $\sigma_c$ .

The evolution of the normalized histograms as a function of system size is shown in Fig. 9. One can see that the distributions are wide and rather complicated. On the one hand, there is a well-defined peak on the right-hand side of the histograms whose height increases and width decreases as  $N$  increases. This peak, however, does not exist for  $\sigma < \sigma_c$  when  $m$  is in the range of the infinite avalanche (for instance  $m = 0.68$  in the left panel of the figure). On the other hand, there is another contribution which extends over a finite range and which is almost size-independent: it is responsible for the fact that the field is not self-averaging. By analyzing the sequence of microscopic states along each  $M$ -driven trajectory, we have checked that these two contributions come from the stable and unstable states, respectively. Since they are no other stable states than those belonging to the  $H$ -driven magnetization curve in the thermodynamic limit (as shown in Fig. 3), we therefore conjecture that the distribution  $P_N(H; m)$  has the following asymptotic form:

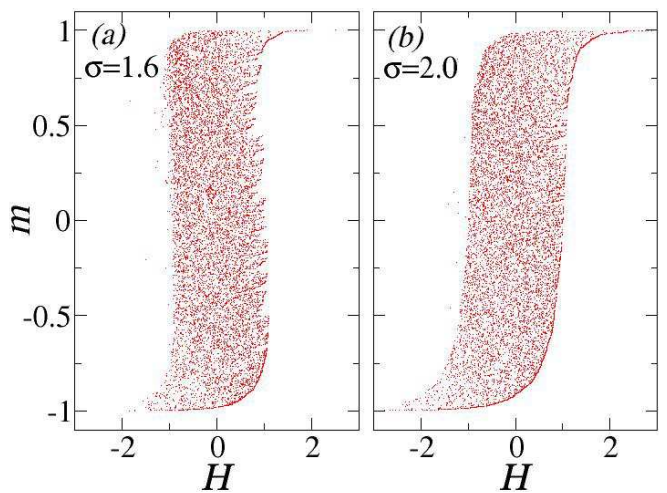


FIG. 8: (Color on line) Ascending branch of the  $M$ -driven trajectory in the field-magnetization plane. Data correspond to a single disorder realization on a random graph with connectivity  $z = 4$  ( $N = 10^4$ ).

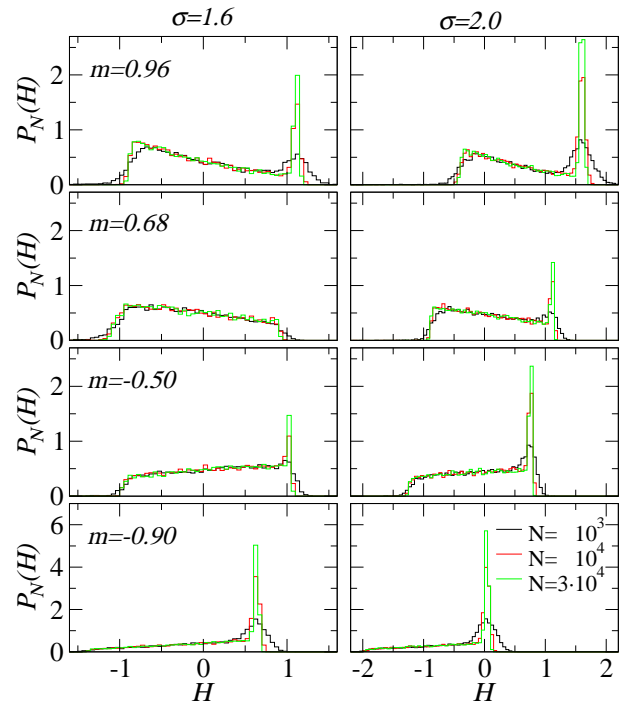


FIG. 9: (Color on line) Normalized histograms of the output field  $H$  for selected values of  $m$  and different system sizes. The data correspond to  $10^4$  disorder realizations.

$$P_\infty(H; m) = Q(m)\delta(H - \hat{H}) + [1 - Q(m)]w(H; m) \quad (16)$$

where  $\delta(H)$  is the Dirac function,  $\hat{H}(m)$  is the field along the magnetization curve (i.e. the field taken as a function of the magnetization), and  $w(H; m)$  is a continuous



distribution on a finite interval  $\{H_{min}(m), H_{max}(m)\}$ . Moreover, there is strong numerical evidence that  $H_{max}(m) = \hat{H}(m)$  for  $\sigma > \sigma_c$  and for  $\sigma < \sigma_c$  outside the range of the macroscopic avalanche, whereas  $H_{max}(m) < \hat{H}(m)$  inside the infinite avalanche.

The statistical behavior of the field for a given value of the magnetization is thus different above and below  $\sigma_c$ . For  $\sigma > \sigma_c$ , the most probable value of  $H(m)$  is the one corresponding to the  $H$ -driven magnetization curve (the two protocols thus give the same field-magnetization diagram), but there is a finite probability that it takes a smaller value. For  $\sigma < \sigma_c$  and  $m$  inside the range of the infinite avalanche, one has  $Q(m) = 0$  and the delta peak disappears. In this case, the value of the field is unpredictable inside a finite interval.

#### IV. RESULTS FOR THE CUBIC LATTICE

Very similar results are obtained on the 3-D cubic lattice. In this case, however, the  $H$ -driven behavior cannot be treated exactly in the thermodynamic limit and one must also perform simulations on finite systems.

Fig. 10 shows the fraction of stable states along the  $M$ -driven trajectory. The curves are similar to the ones displayed in Fig. 4 except for a stronger asymmetry. Again, one finds that  $Q(m) = 0$  when  $m$  is in the range of the  $H$ -driven macroscopic avalanche below  $\sigma_c$ .

Fig. 11 shows that the internal energy obtained with the  $M$ -driven algorithm is still a self-averaging quantity both above and below  $\sigma_c$  ( $\sigma_c \simeq 2.2$ ). However, it seems that the variance decreases slower than  $1/L^3$  when  $m$  is in the range of the infinite avalanche, a behavior also observed Ref.[7] although the definition of the field is quite different.

The comparison between the two algorithms for the average internal energy as a function of  $m$  is performed in Fig. 12. Note that there is again a double well structure at low disorder but the two minima are very close to  $m = \pm 1$  and hardly visible on the figure. There is only one minimum below  $\sigma \approx 3$ , a value quite different from  $\sigma_c$ . It seems again that the two algorithms give the same energy in the thermodynamic limit (outside the infinite avalanche) but the finite-size effects are more important than on the Bethe lattice. Finally, the histograms of the field  $H(m)$  are shown in Fig. 13. The overall behavior is similar the one displayed in Fig. 9 and we thus conjecture that the asymptotic form of the probability distribution is given by Eq. (18). Note however that the continuous part  $w(H; m)$  has a very different shape than on the Bethe lattice.

#### V. DISCUSSION

In the present paper, we have proposed a simple modification of the standard single-spin-flip algorithm to study the magnetization-driven RFIM at  $T = 0$ . The

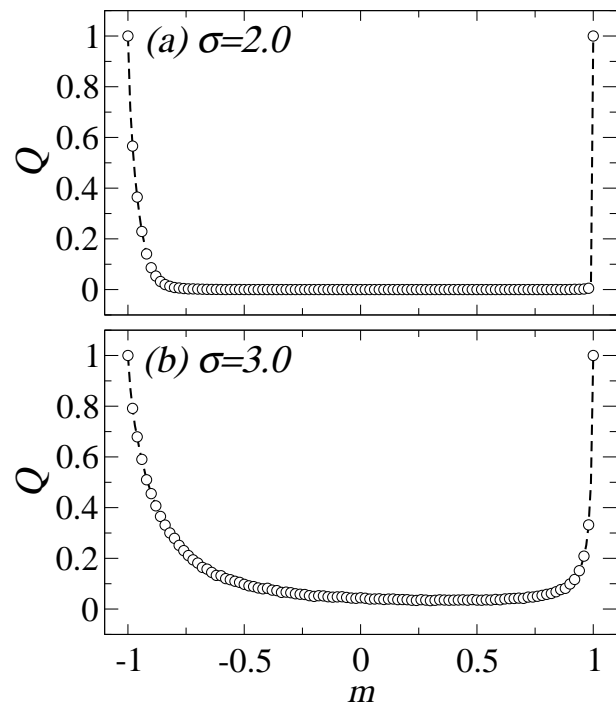


FIG. 10: Fraction  $Q(m)$  of stable states along the  $M$ -driven trajectory on a cubic lattice (only the ascending branch is shown). The lattice size is  $L = 30$  and the average has been taken over  $3 \times 10^4$  disorder realizations. Lines are guides to the eye.

dynamics consists in flipping the spins one by one, choosing the spin with the largest local field. This allows to perform a detailed comparison with the microscopic trajectory of the system in the  $H$ -driven situation, above and below the critical disorder. It turns out that the two trajectories share the same metastable states in the thermodynamic limit, and we have computed the average fraction of these states. An exact expression of this quantity has been obtained in the case of the Bethe lattice. Numerical simulations show that the two dynamics yield the same internal energy for a given value of the magnetization outside the range of the macroscopic avalanche. On the Bethe lattice, inside the macroscopic avalanche, the energy obtained with the  $M$ -driven algorithm also coincides with the one that can be computed analytically in the  $H$ -driven case, using the solution of the self-consistent equations that describes the unstable branch of the hysteresis loop.

The  $M$ -driven field-magnetization diagram exhibits some peculiar and annoying features that are due to our definition of the output field  $H$  as  $\Delta U/\Delta M$ : i) all closed loops have zero area, implying that there is no dissipation in the system; ii)  $H$  strongly fluctuates with  $m$  and these fluctuations are independent of the system size; iii) the sample-to-sample fluctuations of  $H$  also do not decrease with the system size. We have shown that this problem is related to the presence of a continuous part in the prob-

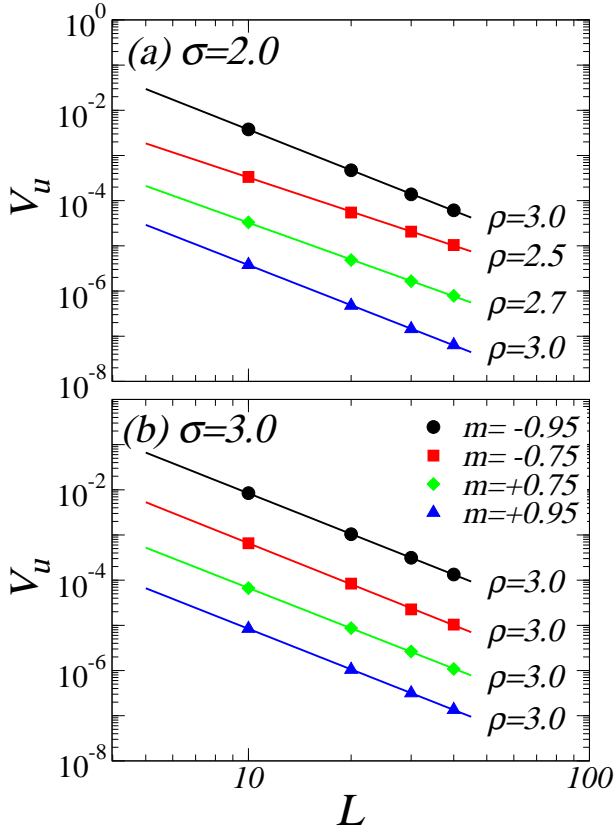


FIG. 11: (Color on line) Variance  $V_u(m)$  of the internal energy per spin  $u(m)$  on the cubic lattice for selected values of  $m$  as a function of system size. Averages are performed over  $3 \times 10^4$  disorder realizations. For the sake of clarity, the variances for  $m = -0.75$ ,  $m = 0.75$  and  $m = 0.95$  are divided by 10, 100 and 1000 respectively. The lines are fits to the form  $V_u(m) \sim L^{-\rho}$ .

ability distribution of  $H$ , which corresponds to the field associated to the unstable states. We now discuss some possible modifications in the definition of the dynamics or of the field.

The first one is to allow for an additional relaxation of the system using the Kawasaki dynamics, which is the standard dynamics for a situation with a conserved order parameter. Specifically, one could imagine to first flip the spin with the largest local field (so to change  $M$ ) and then perform all possible exchanges between nearest-neighbor spins of opposite sign that decrease the energy. This procedure is certainly more in the spirit of the local mean-field calculations that have been performed in Ref.[7] at finite temperature. Even without changing the definition of the field, one may hope that the fluctuations of  $H$  with  $M$  will be weaker and will perhaps decrease with  $N$ . However, preliminary simulations show that the energy of some states cannot be decreased by exchanging nearest-neighbor spins and that many of the final states are still unstable with respect to the (Glauber) single-spin-flip dynamics. It would be interesting to perform an

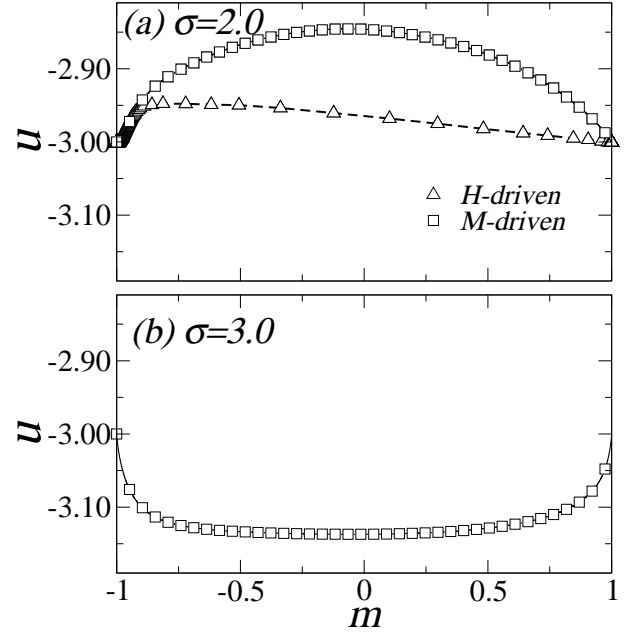


FIG. 12: Average internal energy per spin on the cubic lattice below and above  $\sigma_c$ . The symbols represent the results of the simulation of a system with size  $L = 30$  with the  $H$ -driven and  $M$ -driven algorithms, as indicated. Averages are taken over  $3 \times 10^4$  disorder realizations. Lines are guides to the eye.

extensive study in order to understand if this behavior changes when increasing the system size. On the other hand, it must be emphasized that the stable states are now different from the ones visited by the  $H$ -driven dynamics. Moreover, this procedure does not solve the problem of the definition of the field (and the corresponding absence of dissipation).

A second possibility is to keep the same dynamics as in this work, but to change the definition of the output field. Indeed, it is very likely that the magnetization (or any other extensive variable) can only be controlled at the macroscopic level within a certain resolution. For instance, in an experiment performed at a constant rate  $dM/dt$ , one probably measures not the instantaneous force (in the present case  $-f_i^{max}(m)$ ) but some average  $\bar{H}$  over a certain range  $\Delta m$  (which could even depend on the driving rate). In this case, one can easily check that all fluctuations are suppressed in  $\bar{H}$  in the thermodynamic limit since imposing a fixed resolution  $\Delta m$  implies to take averages over larger and larger intervals  $\Delta M$  when increasing  $N$ .  $\bar{H}$  is then also self-averaging. One may also imagine that the apparatus that measures the field (or the force) cannot adjust itself to the force infinitely fast or that there is some threshold value. Of course, in all these cases, the results are machine-dependent. Careful “ $M$ -driven” experiments with different set-ups and different driving rates are thus needed in order to better resolve these issues.

Finally, from a theoretical point of view, one cannot

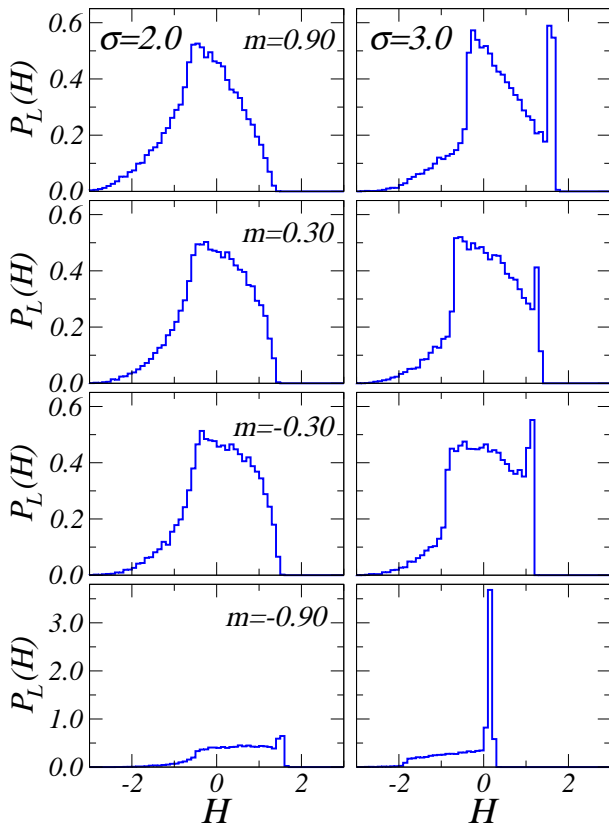


FIG. 13: (Color on line) Normalized histograms of the output field  $H$  for selected values of  $m$  and different system sizes. The data correspond to  $3 \times 10^4$  disorder realizations of a system with size  $L = 30$ .

discard the possibility that there does not exist any satisfactory definition of the output field when using Ising variables. An alternative approach using continuous variables has been proposed in Ref.[7].

### Acknowledgments

The authors acknowledge fruitful discussions with F. J. Perez-Reche, A. Planes, J. P. Sethna, Ll. Mañosa and G. Tarjus. This work has received financial support from CICYT (Spain), project MAT2004-1291 and CIRIT (Catalonia), project 2005SGR00969. Xavier Illa acknowledges financial support from the Spanish Ministry of Education, Culture and Sports. P. Shukla and M. L. Rosinberg thank the Generalitat de Catalunya for financial support (2004PIV2-2, 2005PIV1-17) and the hospitality of the ECM department of the University of Barcelona. The Laboratoire de Physique Théorique de la Matière Condensée is the UMR 7600 of the CNRS.

- 
- [1] J.P.Sethna, K.A.Dahmen, and O.Perković in *The Science of Hysteresis*, edited by G.Bertotti and I.Mayergoyz, Elsevier (2004).
  - [2] Q.Michard and J.P.Bouchaud, *Eur. Phys. J. B* **47**, 151 (2005).
  - [3] K.Otsuka and C.M.Wayman in *Shape Memory Materials*, edited by K.Otsuka and C.M.Wayman, Cambridge University Press, Cambridge (1998).
  - [4] W.Grosse-Nobis, *J. Mag. Mag. Mater.* **4**, 247 (1977).
  - [5] E.Bonnot, Ll.Mañosa, A.Planes, R.Romero, and E.Vives (in preparation).
  - [6] J.P.Sethna, K.Dahmen, S.Kartha, J.A.Krumhansl, B.W.Roberts, and J.D.Shore, *Phys. Rev. Lett.* **70**, 3347 (1993).
  - [7] X.Illa, M.L.Rosinberg, and E.Vives, preprint cond-mat/0607069.
  - [8] D.Dhar, P.Shukla, and J.P.Sethna, *J. Phys. A: Math. Gen.* **30** 5239 (1997).
  - [9] S.Sabhapandit, P.Shukla, and D.Dhar, *J. Stat. Phys.* **98** 103 (2000).
  - [10] X.Illa, J.Ortín and E.Vives, *Phys. Rev. B* **71**, 184435 (2005).
  - [11] O.Perković, K.A.Dahmen and J.P.Sethna, *Phys. Rev. B* **59**, 6106 (1999).
  - [12] F.J.Perez-Reche and E.Vives, *Phys. Rev. B* **67**, 134421 (2003).
  - [13] E.Vives, M.L.Rosinberg, and G.Tarjus, *Phys. Rev. B* **71**, 134424 (2005).
  - [14] F.Detcheverry, M.L.Rosinberg, and G.Tarjus, *Eur. Phys. J. B* **44**, 327 (2005).
  - [15] K.Sneppen, *Phys. Rev. Lett.* **69**, 3539 (1992); P.Bak and K.Sneppen, *Phys. Rev. Lett.* **71**, 4083 (1992), M.Paczuski, S.Maaslov, and P.Bak, *Phys. Rev. E* **53**, 414 (1996).
  - [16] R.Brout, *Phys. Rev.* **115**, 824 (1959).
  - [17] K.Binder and D.W.Heermann, *Monte Carlo Simulations in Statistical Physics*, Springer-Verlag, Berlin (1988).
  - [18] X.Illa, P.Shukla, and E.Vives, *Phys. Rev. B* **73**, 092414 (2006).